

Increasing Leidenfrost point using micro-nano hierarchical surface structures

Hyuk-min Kwon, James C. Bird, and Kripa K. Varanasi

Citation: [Applied Physics Letters](#) **103**, 201601 (2013); doi: 10.1063/1.4828673

View online: <http://dx.doi.org/10.1063/1.4828673>

View Table of Contents: <http://scitation.aip.org/content/aip/journal/apl/103/20?ver=pdfcov>

Published by the [AIP Publishing](#)

Articles you may be interested in

[Drop spreading at the impact in the Leidenfrost boiling](#)

Phys. Fluids **27**, 063302 (2015); 10.1063/1.4922066

[Separate effects of surface roughness, wettability, and porosity on the boiling critical heat flux](#)

Appl. Phys. Lett. **103**, 024102 (2013); 10.1063/1.4813450

[Structured surfaces for enhanced pool boiling heat transfer](#)

Appl. Phys. Lett. **100**, 241603 (2012); 10.1063/1.4724190

[Boiling point determination using adiabatic Gibbs ensemble Monte Carlo simulations: Application to metals described by embedded-atom potentials](#)

J. Chem. Phys. **135**, 224113 (2011); 10.1063/1.3665457

[Making human enamel and dentin surfaces superwetting for enhanced adhesion](#)

Appl. Phys. Lett. **99**, 193703 (2011); 10.1063/1.3660579

The advertisement features a blue background with a molecular structure of spheres. On the left is a thumbnail of an 'Applied Physics Reviews' journal cover showing a 3D grid structure. The main text reads 'NEW Special Topic Sections' in large white letters. Below this, it says 'NOW ONLINE' in yellow, followed by 'Lithium Niobate Properties and Applications: Reviews of Emerging Trends' in white. The AIP Applied Physics Reviews logo is in the bottom right corner.

NEW Special Topic Sections

NOW ONLINE
Lithium Niobate Properties and Applications:
Reviews of Emerging Trends

AIP Applied Physics Reviews

Increasing Leidenfrost point using micro-nano hierarchical surface structures

Hyuk-min Kwon,¹ James C. Bird,² and Kripa K. Varanasi^{1,a)}

¹*Department of Mechanical Engineering, Massachusetts Institute of Technology, Cambridge, Massachusetts 02139, USA*

²*Department of Mechanical Engineering, Boston University, Boston, Massachusetts 02155, USA*

(Received 3 July 2013; accepted 8 September 2013; published online 11 November 2013)

The Leidenfrost effect is undesirable in cooling applications as the vapor layer on which the liquid levitates acts as a heat transfer barrier. Here, we report on increasing the Leidenfrost temperature by surface textures that can promote droplet wetting at high superheat via capillary wicking. Counterintuitively, we find that sparser rather than denser textures increase the Leidenfrost temperature. Our experimental results are consistent with a physical model that balances capillary wetting pressures with dewetting pressures exerted by the escaping vapor. The physical mechanism suggests that hierarchical textures have a higher Leidenfrost temperature compared to single-length-scale textures, which is confirmed experimentally. © 2013 AIP Publishing LLC. [<http://dx.doi.org/10.1063/1.4828673>]

Boiling of liquids is widespread in many applications such as power generation, refrigeration, desalination, chemical processing, and electronics cooling.^{1–4} Recently, there has been significant interest in enhancing pool boiling, where the heated surface lies immersed in a large volume of stagnant liquid, using micro/nanostructured^{5–11} and hybrid surfaces.^{12–15} Another important class of boiling situations involves rapid cooling or quenching of overheated components using droplet impingement, sprays, or by plunging into a liquid;¹⁶ applications of spray cooling include cooling of nuclear fuel rods,¹⁷ fire suppression,¹⁸ high-flux thermal management of electronic and photonic devices,¹⁹ and metallurgical processes.²⁰ Cooling is effective when liquid droplets are able to come into direct contact with the solid surface. However, when the surface temperatures are above the Leidenfrost point (LFP), liquid droplets levitate, and contact with the surface is lost due to the formation of a vapor layer.^{21,22} The vapor layer acts as a thermal barrier and significantly limits the heat transfer from the hot solid to the liquid coolant.¹ Under such conditions, cooling is ineffective and the temperature of the substrate can reach dangerous levels, such as those experienced in the Fukushima disaster.^{23,24} Hence, higher LFP is desirable for enhancing cooling of overheated components.

Prior studies on increasing LFP include modifying the chemical properties of the liquid,^{25–29} surface properties,^{30–38} varying Weber number,^{39–41} and the use of an electric field.⁴² Modifying the surface is particularly attractive because liquid properties and other operational conditions are often constrained. Although most previous studies have identified surface roughness as an important property that generally leads to an increase in LFP,^{30–37} there are occasional studies that show this trend is perhaps in the reverse direction.^{38,43} These studies, although informative, have been limited to random roughness substrates such as porous ceramics,^{31,32} particle blasted and rough sanded,³⁴

salt deposited,³⁵ and particle coated.³⁶ As a result, the effects of surface texture on LFP are not easily quantifiable, and the physical mechanisms governing the phenomenon remain largely unclear. Here, we carry out systematic experiments, which show that surface texture does not always increase LFP. We reveal a more complex picture where competition between texture-induced capillary pressures and dewetting vapor pressures influences LFP and provide important insights for increasing LFP using hierarchical textures.

The effect of surface texture on the LFP is investigated by depositing millimetric droplets (30 μl , deionized water) onto heated silicon surfaces textured with arrays of micro-scale silicon square posts (Fig. 1).⁴⁴ Drops are gently deposited to minimize inertial effects ($We \sim 1$). The Weber number is defined as $We = \rho_L U^2 R / \gamma$, where ρ_L is the density of liquid, U is the impinging velocity, R is the radius of droplets, and γ is the surface tension of the liquid. The post surfaces are fabricated using standard lithography techniques with post width $a = 10 \mu\text{m}$, height $h = 10 \mu\text{m}$, and edge-to-edge spacing b ranging from $3.3 \mu\text{m}$ to $100 \mu\text{m}$.⁴⁴ For comparison, a smooth silicon surface without texture is also studied. All of the surfaces are subjected to Piranha cleaning⁴⁵ such that water droplets completely spread on the surfaces at room temperature (contact angle $\sim 0^\circ$). The LFP is determined by increasing the surface temperature in small increments and observing droplets transition from vigorous boiling to Leidenfrost state using a high-speed camera. For the smooth silicon surface the LFP is found to be between 270°C (a drop vigorously boils) and 300°C (a drop floats on the surface) as shown in Fig. 1(a) and consistent with the previous studies.³⁶

Interestingly, on textured surfaces, we found the LFP to be higher on surfaces with sparser rather than denser post spacings. For example, the LFP on a textured surface with post spacing $b = 10 \mu\text{m}$ was similar to that on a non-textured surface (Fig. 1(b)). However, when the post spacing was increased to $b = 75 \mu\text{m}$, the drop boils at both 270°C and 300°C (Fig. 1(c)), indicating that the LFP is higher on the sparser surface. Careful measurements of the transition from

^{a)}Author to whom correspondence should be addressed. Electronic mail: varanasi@mit.edu

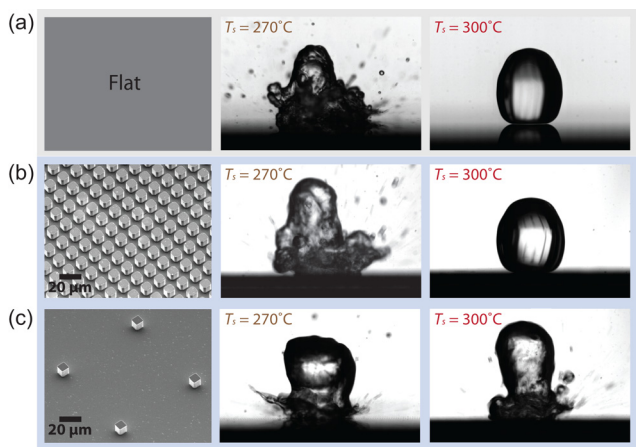


FIG. 1. Effects of surface texture on drop dynamics at two different surface temperatures, T_s . (a) At $T_s = 270^\circ\text{C}$ (left), a deionized water drop spreads on the surface, and at the same time vigorously boils, ejecting smaller drops. At $T_s = 300^\circ\text{C}$ (right), a water drop floats on the surface without experiencing significant phase change known as the Leidenfrost effect. The Leidenfrost transition temperature (LFP) lies between 270°C and 300°C . (b), (c) Liquid droplets on micropost arrays ($a = 10\ \mu\text{m}$, $h = 10\ \mu\text{m}$) with spacings $b = 10\ \mu\text{m}$ and $b = 75\ \mu\text{m}$, respectively, at the same two temperatures. The LFP hardly changes with the dense post array, while the sparse post array promotes boiling by preventing the Leidenfrost effect (enhanced online) [URL: <http://dx.doi.org/10.1063/1.4828673.1>].

contact to floating states are presented in Fig. 2(a), where closed symbols depict contact and boiling, while open symbols depict flotation and Leidenfrost state. The LFP is therefore the transition temperature between the two regimes. Inspection of Fig. 2(a) indicates that as the post array becomes denser ($b \rightarrow 0$), the LFP of a textured surface approaches that of a flat surface. As the array becomes sparser (as b increases), the LFP increases, reaching a value of $\sim 370^\circ\text{C}$ for a spacing of $b = 100\ \mu\text{m}$. This result is surprising because common knowledge would suggest that denser textures should result in higher LFP as they can facilitate enhanced wetting due to higher capillary forces.⁴⁶

To rationalize these experimental findings, we propose the following model. A drop that is in contact with the textured surface must detach if it is to float on its own vapor. We hypothesize that while the drop is in contact with the surface, it is subject to two competing processes (Figs. 2(b) and 2(c)). Specifically, capillary forces from the textured surface act to maintain contact by pulling the interface downwards while compressive forces from the vapor generated by the drop push the interface upwards. If these two competing mechanisms dominate the dynamics, then the drop will transition from wetting to floating when the force pushing it upward is comparable to the force pulling it downward. Using the schematic in Figs. 2(b) and 2(c) as a guide, we now estimate these competing forces.

In our experiments, drops are gently deposited on the substrate ($We \sim 1$); however, even this gentle deposition can cause impalement into the micropost array.⁴⁷ The micropost array is hot enough that some of the impaled liquid quickly evaporates, creating a liquid-vapor interface. Because the solid surface is intrinsically highly wetting (i.e., intrinsic contact angle $\sim 0^\circ$), we expect the liquid that is in contact with the surface to form menisci as shown in Figs. 2(b) and 2(c). The characteristic curvature of the interface leads to a

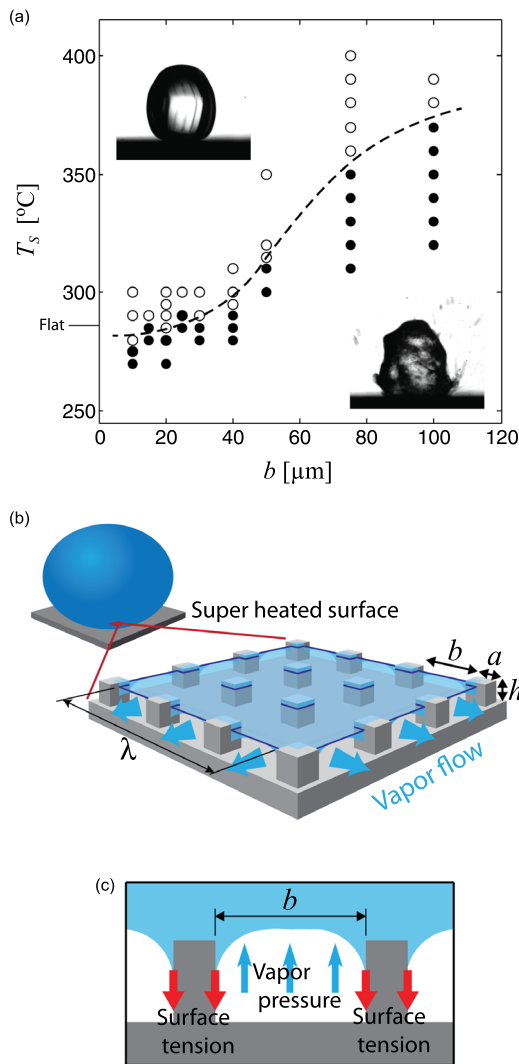


FIG. 2. (a) Experimental results of wetting and non-wetting drops from the micropost arrays with different spacings. Wetted boiling drops are denoted as closed circle markers, and a non-wetting Leidenfrost drops as open circle markers. The dashed line is only for visual clarity. (b) and (c) Schematic representation of the liquid interface on a textured surface at an elevated temperature. (b) As liquid comes into contact with the surface, it spreads through hydrophilic solid features while rapidly evaporating at the interface due to super heat from the solid. The vapor starts to find paths to escape and the posts resist the flow resulting in a pressure differential. (c) Finally, continuous re-wetting through the surface features is possible when the capillary pressure overcomes the pressure from the flowing vapor.

capillary pressure $\Delta P_{cap} \sim \gamma/b$, where γ is the surface tension between the liquid and the vapor. The capillary pressure leads to a force that pulls the interface downwards into the micropost array; the strength of this capillary adhesion increases as the spacing between the posts b decreases.

There is a competing force pushing up on the drop due to the compressive pressure from the vapor under the drop. As the drop evaporates, the vapor under the drop pressurizes to the point where it can drive an outward flow. The surface texture hinders this outward vapor flow and therefore to achieve the same flow rate in the presence of texture requires a larger pressure differential. The pressure under the drop can be estimated by modeling the vapor flow as a viscous-dominated radial Poiseuille flow.^{31,48} There are two components of shear loss for the vapor flow: one associated with the gradient of velocity across the height e of the vapor layer

and the other with that across the spacing b between the posts.⁴⁹ The former component scales as $\mu_v V/e^2$ while the latter scales as $\mu_v V/b^2$, where μ_v is the dynamic viscosity and V is the velocity of vapor. Therefore, the pressure gradient along the flow dP_{vap}/dr is a combination of both the terms and scales as $\mu_v V/K$, where $K = (1/e^2 + 1/b^2)^{-1}$ is the approximate permeability. Because the flow rate is generated from evaporation, the value of V can be approximated using energy balance.⁴⁸ The mass flow rate of vapor per unit width $dm_{vap}/dt \sim \rho_v V e$ is balanced with that of evaporation per unit width resulting from heat transfer through the gap $dm_{evap}/dt \sim q\lambda/h_{fg}$, where ρ_v is the vapor density, q is the heat flux, h_{fg} is the latent heat of vaporization, and λ is the length of the contact patch that is in contact with the surface. Therefore, the force per unit area pushing upward on the drop under a contact patch of length λ scales as $\Delta P_{vap} \sim (\mu_v q \lambda^2)/(\rho_v h_{fg} e K)$.

The conductive heat flux q from the hot surface can be expressed as $q = k_{eff} \Delta T/e$, where ΔT is the temperature difference between the substrate temperature T_s and the saturation temperature T_{sat} . The effective thermal conductivity k_{eff} can be related to the micropost geometry by approximating the parallel solid and vapor thermal paths between the drop and the substrate. Hence, the effective thermal conductivity is modeled as $k_{eff} = (k_v((1 + b/a)^2 - 1) + k_s)/(1 + b/a)^2$, where k_v and k_s are the conductivities of the vapor and solid, respectively.

In our model, the transition to the Leidenfrost state occurs when the pressure exerted by the flowing vapor overcomes the texture-induced capillary pressure. At this transition point, the thickness of the vapor is approximately equal to the height of the microposts, $e \approx h$. It has been observed that the interface near transition is composed of numerous dynamic pinning and depinning regions under the drop.³⁶ These perturbations lead to capillary waves throughout the drop and ejection of small satellite droplets. The size of these droplets is comparable to the wavelength of these perturbations and thus comparable to the length of the local contact patch. We measured the size of these droplets near LFP and found that the diameter was approximately $60 \mu\text{m}$. Therefore, we approximate the contact patch length at transition in our physical model as $\lambda^* \sim 60 \mu\text{m}$ (Fig. 2(b)).

Our physical model predicts that the transition to the Leidenfrost state occurs when $\Delta P^*_{vap}/\Delta P_{cap} \sim 1$. For the heated, micropost array, this pressure balance can be expressed in terms of the texture spacing as $\Delta P^*_{vap}/\Delta P_{cap} \sim (\mu_v k_{eff} \Delta T^* \lambda^{*2} b)/(\rho_v h_{fg} h^2 K \gamma)$, where ΔT^* is the difference between the substrate temperature and saturation temperature at LFP. We calculate the values of this ratio using the experimentally measured transition temperatures for different micropost arrays (Fig. 2(a)) and indeed find that $\Delta P^*_{vap}/\Delta P_{cap}$ is of order one (Fig. 3). We observe that there is a slight dependence with b/λ^* in Fig. 3, which may indicate that one of the parameters that we model as constant, such as λ^* , might also depend on the spacing b . Nevertheless, the overall result that the two pressures are comparable at transition is consistent with our physical model and highlights the dual role of texture. It appears that textures not only elevates the LFP by increasing capillary pressure but also limits the LFP elevation by increasing the resistance to the escaping vapor flow.

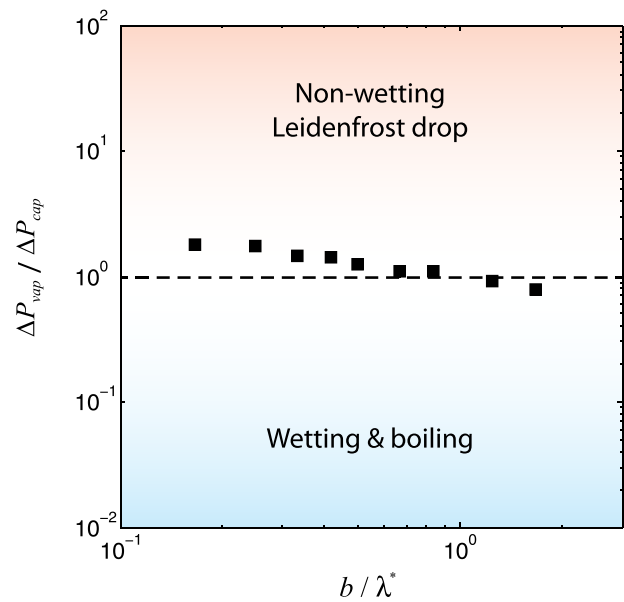


FIG. 3. Vapor pressure normalized by capillary pressure for the experimentally measured LFP, marked as the closed squares, for each different texture, corresponding to the post spacing normalized by the critical contact length, b/λ^* . Our experiments show reasonable match to the line where the capillary wetting pressure balances the compressive vapor pressure, $\Delta P_{vap}/\Delta P_{cap} \sim 1$. The transition to the Leidenfrost state happens when the vapor pressure overcomes the capillary pressure.

If the physical model presented here is correct, it would follow that further elevation of the LFP might be possible if the texture could increase the capillary pressure without increasing the resistance to the escaping vapor flow. This prediction inspired us to develop a hierarchical textured surface, which we fabricated by coating nanoparticles via spin-coating of its colloidal solution (220 nm diameter silica particles) onto a micropost array ($b = 75 \mu\text{m}$).⁴⁴ When we compare the performance of the hierarchical surface at a temperature above the LFP for the non-hierarchical control surfaces, the results are striking (Fig. 4). When the substrates are at 400°C (the limit of our experimental setup), an impacting drop will float above both a surface with a single micro-scale texture ($b = 75 \mu\text{m}$; Fig. 4(a)) and a surface with a single nano-scale texture ($b = 800 \text{ nm}$; Fig. 4(b)). However, when a drop impacts the micro-nano hierarchical surface texture heated to the same temperature, the drop rapidly wets the surface demonstrating that the LFP has been significantly elevated (Fig. 4(c)). All three results are consistent with the mechanisms in our physical model when the wetting depends on the smallest texture length scale and vapor resistance depends on the largest texture length scale. Other factors may also contribute to this effect, such as nucleation site density increment, and local compressibility, which may change the escaping vapor pressure and the vaporization temperature of a liquid. Nevertheless, our experimental results and physical model provide insight into how surface texture design can have a profound effect on the LFP.

In summary, we show that Leidenfrost point on textured surfaces occurs when capillary pressures balance compressive pressures exerted by the vapor. For single-length scale nano- or micro- textures, we show that texture can not only elevate LFP by increasing capillary pressure but also limit the LFP elevation by increasing the resistance to the

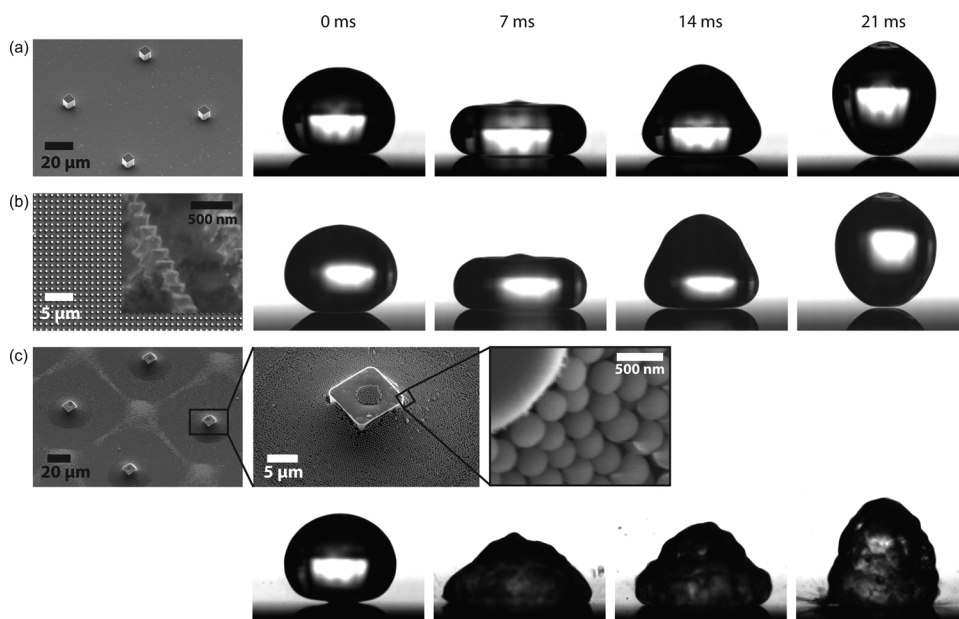


FIG. 4. High speed image sequences of liquid drop behaviors on 400 °C surfaces with three different surface structures: (a) and (b) are single-length scale textures while (c) is a hierarchical texture. (a) Micro-scale surface structure, ($a = 10 \mu\text{m}$, $h = 10 \mu\text{m}$) with spacings $b = 75 \mu\text{m}$. (b) Nano-scale surface structure, 200 nm diameter circular pillar array with 800 nm spacing. (c) Micro-nano hierarchical surface structure, with $a = 10 \mu\text{m}$ and $h = 10 \mu\text{m}$ micropost array with spacing $b = 75 \mu\text{m}$, covered with nano-particles (220 nm diameter). The hierarchical structure, unlike those in (a) and (b), promotes droplet wetting and boiling at 400 °C (enhanced online) [URL: <http://dx.doi.org/10.1063/1.4828673.2>].

escaping vapor flow. We show that further increase in LFP can be achieved using hierarchical micro-nano textures as they can significantly increase the capillary pressures without additional resistance to the vapor flow. These insights can be used to enhance the heat transfer performance in various cooling applications, including cooling of nuclear fuel rods under transient and accident conditions, fire suppression, electronics cooling, and metallurgy.

We gratefully acknowledge the support from DARPA Young Faculty Award, MIT Energy Initiative, and the MIT-Deshpande Center. We also thank the Microsystems Technology Lab (MTL) at MIT and the Center for Nanoscale Systems (CNS) at Harvard University. We thank Adam Paxson for help with developing the cover image for this issue (11 November 2013, vol. 103, issue 20).

¹V. P. Carey, *Liquid-Vapor Phase-Change Phenomena* (Taylor & Francis Group, LLC, New York, NY, 1992).

²W. M. Rohsenow, J. P. Hartnett, and Y. I. Cho, *Handbook of Heat Transfer* (McGraw-Hill, New York, 1998).

³V. K. Dhir, *Annu. Rev. Fluid Mech.* **30**(1), 365 (1998).

⁴N. A. Patankar, *Soft Matter* **6**(8), 1613 (2010).

⁵S. Launay, A. G. Fedorov, Y. Joshi, A. Cao, and P. M. Ajayan, *Microelectron. J.* **37**(11), 1158 (2006).

⁶R. Chen, M.-C. Lu, V. Srinivasan, Z. Wang, H. H. Cho, and A. Majumdar, *Nano Lett.* **9**(2), 548 (2009).

⁷C. Li, Z. Wang, P.-I. Wang, Y. Peles, N. Koratkar, and G. P. Peterson, *Small* **4**(8), 1084 (2008).

⁸Y.-W. Lu and S. G. Kandlikar, *Heat Transfer Eng.* **32**(10), 827 (2011).

⁹K.-H. Chu, R. Enright, E. N. Wang, *Appl. Phys. Lett.* **100**, 241603 (2012).

¹⁰I. U. Vakarelski, N. A. Patankar, J. O. Marston, D. Y. C. Chan, and S. T. Thoroddsen, *Nature* **489**(7415), 274 (2012).

¹¹J. A. Weibel, S. S. Kim, T. S. Fisher, and S. V. Garimella, *Nanoscale Microscale Thermophys. Eng.* **16**(1), 1 (2012).

¹²A. R. Betz, J. Xu, H. Qiu, and D. Attinger, *Appl. Phys. Lett.* **97**(14), 141909 (2010).

¹³H. Jo, H. S. Ahn, S. Kang, and M. H. Kim, *Int. J. Heat Mass Transfer* **54**(25–26), 5643 (2011).

¹⁴S. P. R. Kobaku, A. K. Kota, D. H. Lee, J. M. Mabry, and A. Tuteja, *Angew. Chem., Int. Ed.* **51**(40), 10109 (2012).

¹⁵A. R. Betz, J. Jenkins, C.-J. C. Kim, and D. Attinger, *Int. J. Heat Mass Transfer* **57**(2), 733 (2013).

¹⁶J. Kim, *Int. J. Heat Fluid Flow* **28**(4), 753 (2007).

¹⁷H. van Dam, *Rep. Prog. Phys.* **55**, 2025 (1992).

¹⁸G. Grant, J. Brenton, and D. Drysdale, *Prog. Energy Combust. Sci.* **26**(2), 79 (2000).

¹⁹S. V. Garimella, A. S. Fleischer, J. Y. Murthy, A. Keshavarzi, R. Prasher, C. Patel, S. H. Bhavnani, R. Venkatasubramanian, R. Mahajan, and Y. Joshi, *IEEE Trans. Compon. Packag. Technol.* **31**(4), 801 (2008).

²⁰J. D. Bernardin and I. Mudawar, *Int. J. Heat Mass Transfer* **38**(5), 863 (1995).

²¹J. G. Leidenfrost, *De aquae communis nonnullis qualitatibus tractatus* (Ovenius, Duisburg, Germany, 1756).

²²D. Quéré, *Annu. Rev. Fluid Mech.* **45**(1), 197 (2013).

²³J. Buongiorno, R. Ballinger, M. Driscoll, B. Forget, C. Forsberg, M. Golay, M. Kazimi, N. Todreas, and J. Yanch, *Technical Lessons Learned from the Fukushima-Daichii Accident and Possible Corrective Actions for the Nuclear Industry: An Initial Evaluation* (MIT Center for Advanced Nuclear Energy Systems, Cambridge, MA, 2011).

²⁴G. Brumfiel, "Fukushima crisis: Anatomy of a meltdown," Nature News Blog (13 March 2011), available at http://blogs.nature.com/news/2011/03/fukushima_crisis_anatomy_of_a.html.

²⁵C. Avedisian and M. Fatehi, *Int. J. Heat Mass Transfer* **31**(8), 1587 (1988).

²⁶Y. M. Qiao and S. Chandra, *Proc. R. Soc. Lond. A* **453**(1959), 673–689 (1997).

²⁷V. Bertola, *Exp. Fluids* **37**, 653 (2004).

²⁸V. Bertola, *Int. J. Heat Mass Transfer* **52**(7–8), 1786 (2009).

²⁹G. Duursma, K. Sefiane, and A. Kennedy, *Heat Transfer Eng.* **30**(13), 1108 (2009).

³⁰C. M. Weickgenannt, Y. Zhang, S. S. Ray, I. Roisman, T. G. Roisman, C. Tropea, A. L. Yarin, *Phys. Rev. E* **84**, 036310, (2011).

³¹C. Avedisian and J. Koplik, *Int. J. Heat Mass Transfer* **30**(2), 379 (1987).

³²S. Chandra and C. Avedisian, *Int. J. Heat Mass Transfer* **35**(10), 2377 (1992).

³³M. Prat, P. Schmitz, and D. Poulikakos, *J. Fluids Eng.* **117**(3), 519 (1995).

³⁴J. D. Bernardin, C. J. Stebbins, and I. Mudawar, *Int. J. Heat Mass Transfer* **40**(1), 73 (1996).

³⁵Q. Cui, S. Chandra, and S. McCahan, *J. Heat Transfer* **125**(2), 333 (2003).

³⁶H. Kim, B. Truong, J. Buongiorno, and L. W. Hu, *Appl. Phys. Lett.* **98**, 083121 (2011).

³⁷H.-M. Kwon, J. C. Bird, and K. K. Varanasi, *Bull. Am. Phys. Soc.* **56**(18), BAPS.2011.DFD.H6.3 (2011), available at <http://meetings.aps.org/Meeting/DFD11/Session/H6.3>.

³⁸T. Tran, H. J. J. Staat, A. Susarrey-Arce, T. C. Foertsch, A. van Houselt, H. J. G. E. Gardeniers, A. Prosperetti, D. Lohse, and C. Sun, *Soft Matter* **9**, 3272 (2013).

³⁹J. Bernardin, C. Stebbins, and I. Mudawar, *Int. J. Heat Mass Transfer* **40**(2), 247 (1997).

⁴⁰N. Z. Mehdizadeh and S. Chandra, *Proc. R. Soc. London. Ser. A* **462**(2074), 3115 (2006).

⁴¹T. Tran, H. J. J. Staat, A. Prosperetti, C. Sun, and D. Lohse, *Phys. Rev. Lett.* **108**, 036101 (2012).

⁴²F. Celestini and G. Kirstetter, *Soft Matter* **8**, 5992 (2012).

⁴³D. Arnaldo del Cerro, Á. G. Marín, G. R. B. E. Römer, B. Pathiraj, D. Lohse, and A. J. Huis in't Veld, *Langmuir* **28**(42), 15106 (2012).

⁴⁴See supplementary material at <http://dx.doi.org/10.1063/1.4828673> for the experimental methods.

⁴⁵S. D. Senturia, *Microsystem Design* (Kluwer Academic Publishers, Boston, MA, 2001).

⁴⁶D. Quéré, *Annu. Rev. Mater. Res.* **38**, 71 (2008).

⁴⁷H.-M. Kwon, A. T. Paxson, K. K. Varanasi, and N. A. Patankar, *Phys. Rev. Lett.* **106**(3), 036102 (2011).

⁴⁸A. Bianche, C. Clanet, and D. Quéré, *Phys. Fluids* **15**, 1632 (2003).

⁴⁹C. Ishino, M. Reyssat, E. Reyssat, K. Okumura, and D. Quéré, *Europhys. Lett.* **79**, 56005 (2007).